scientific reports

Check for updates

OPEN

Multi-environment and multi-parameter screening of stability and coating efficiency of gold nanoparticle bioconjugates in application media

Junjie Wang[1,3], Stefano Giordani[1,3], Valentina Marassi[1,2]✉, Anna Placci[1], Barbara Roda[1,2], Pierluigi Reschiglian[1,2] & Andrea Zattoni[1,2]

Gold nanoparticles (AuNPs) and their biocompatible conjugates find wide use as transducers in (bio) sensors and as Nano-pharmaceutics. The study of the interaction between AuNPs and proteins in representative application media helps to better understand their intrinsic behaviors. A multi-environment, multi-parameter screening strategy is proposed based on asymmetric flow field flow fractionation (AF4)-multidetector. Citrate-coated AuNPs (AuCIT, 25.1 ± 0.2 nm) and PEG-coated AuNPs (AuPEG, 38.3 ± 0.8 nm) were employed with albumin as a model system. Attention was put in investigating the influence of Au/BSA mass ratios, that allowed to identify the yield-maximizing (1:1) and product-maximizing (2.5:1) conditions for the generation of AuNPs-protein conjugates. Furthermore, bioconjugate properties were thoroughly assessed across various saline media with different pH and ionic strengths. While AuNPs with PEG coating exhibit greater stability at high salinities, such as 30 mM, their conjugates are less stable over time. In contrast, although bare AuNPs are significantly affected by pH and salt concentration, once conjugates are formed, their stability surpasses that of the conjugates formed with AuPEG. The developed methodology can fill the vacancy of standard reference quality control (QC) procedures for bioconjugate synthesis and application in (bio)sensors and Nano-pharmaceutics, screening in a short time many combinations, easily scaling up to the semi-preparative scale or translating to different bioconjugates.

Keywords Gold nanoparticles (AuNPs), Asymmetric flow field flow fractionation (AF4), Bioconjugates, Multi-environment and multi-parameter screening strategy

Gold nanoparticles (AuNPs) emerged arguably as one of the most promising class of nanoparticles for medical and sensor applications due to their outstanding features. They are characterized by extinction coefficients three to five orders of magnitude higher than typical organic dyes making them suitable for the generation of extremely sensitive sensors and for other applications such as photon ablation[1]. They are also characterized by simple surface modification, excellent biocompatibility and high versatility yielding differently sized and shaped NPs. The biological effects of AuNPs (including their (cyto)toxicity and pharmacokinetics) as well as their physical and chemical properties, vary according to their size, shape, and surface modifications[2]: the study of how AuNPs interact with the biological environment represents a necessary requirement in the development of systems within applications in the health and food fields[3]. Moreover, NPs' surface interactions with biologically active components (ex. proteins[4], biotin[5], aptamers[6]) are often involved in AuNPs-based sensors. Due to their hybrid and unique nature, the quality control of those systems poses a series of analytical challenges, since drug loading, particle stability in different media, surface properties and particle interactions with the immune system are far from being fully standardized[7]. Consequently, various analytical techniques have been exploited to examine NPs, their conjugates and associated properties. Examples are ultraviolet-visible spectroscopy[8], fluorescence spectroscopy[9], dynamic light scattering[10], atomic force microscopy[11], size exclusion chromatography (SEC)[12], capillary electrophoresis (CE) steady state quenching titration[13], and circular dichroism[14]. However, most of

[1]Department of Chemistry G. Ciamician, University of Bologna, Bologna 40126, Italy. [2]byFlow srl, Bologna 40129, Italy. [3]Junjie Wang and Stefano Giordani contributed equally to this work. ✉email: valentina.marassi@unibo.it

them work in batch mode and are only able to provide averaged results, while SEC and EC although able to separate the different components of a sample are limited in terms of carriers. Consequently, sometimes it is only possible to perform the measurements in suboptimal conditions which may affect data interpretation and their use in further applications. An improvement is represented by Asymmetrical Flow Field Flow Fractionation (AF4). AF4 is an extremely flexible technique both in terms of mobile phase and sample type that allows to perform a gentle separation of analytes in a broad size range and in native conditions[15]. AF4-multidetection platforms have proven themselves as powerful tools to analyze nanoparticles and metal nanoparticles[16], proteins and antibodies[17,18], aptamers[19], even in complex matrixes[20,21]. AuNPs and their conjugation to aptamers and immunoglobulins have been successfully studied with AF4 [22,23]. Those platforms allowed to study the binding of different species to AuNPs and to monitor the aggregation process involved in binding assays, separating the conjugates from the free components and characterizing them in terms of size, mass, and spectroscopical properties. The result also highlighted the flexibility of the platform in terms of mobile phase usable, allowing to optimize environment for the conjugated system. AF4 characterization of these systems was also obtained by the coupling of the platform with an Inductively coupled plasma mass spectrometry (ICP-MS) detector which provides lower limit of detection (LOD) and allows powerful peak deconvolution to identify different coeluting species, though this approach is expensive and destructive of the sample[24].

Beyond AuNPs synthesis and conjugation, the screening of application conditions and conjugate stability therein, is as fundamental as often unaddressed, and a great part of the literature focuses on one aspect of AuNP production but cannot provide a platform or strategy to translate these materials towards their use. In our work, we aimed at bridging these necessities and evolving from an analytical approach able to represent one condition, to one able to assess many parameters systematically and with minimal operational variation, starting from conjugation efficacy to medium stability. Since albumin is an inexpensive, widely used protein and one of the most abundant ones in biological matrixes of biomedical interest, it was chosen as a model protein to gather information of the interactions with AuNPs presenting different coatings (Citrate and PEG-AuNPs, as two of the most common ones) and proteins in different ratios and medium.

To fulfill this aim, an AF4-multidetection platform including a diode array detector and a multiangle light scattering detector (AF4-DAD-MALS) was implemented for the separation, characterization, and quantification of AuNPs-protein conjugates without pre-purification. These results were rapidly provided in native conditions and were highly reproducible reinforcing the position of AF4-multidetection as a benchmark technique for nanosystems characterization. Aside from the classical spectroscopical/size characterization of the systems, a series of experiments were performed to evaluate the effects of incubation time, pH and ionic strength on NPs-protein binding process and yield, which affect conjugate stability and their effectiveness as biocompatible agents and sensor transducers. With a careful experiment design, it was possible for the first time to evaluate the presence of equilibrium processes affecting the conjugation and obtain information concerning the stoichiometry of the complexes.

Materials and methods

Materials

Gold (III) chloride trihydrate (HAuCl4·3H2O, ≥ 49.0% Au basis), Sodium citrate ($C_6H_5Na_3O_7$, ≥ 98.0%), Sodium phosphate dibasic dihydrate (Na_2HPO_4 * 2 H_2O, ≥ 99.0%), Sodium phosphate monobasic dihydrate (NaH_2PO_4 * 2 H_2O, ≥ 99.0%), Poly(ethylene glycol) methyl ether thiol (5000 g/mol), and Bovine serum albumin (BSA, ≥ 98.0%) were purchased by Sigma Aldrich (St. Louis, MO, USA). All AuNPs solutions were prepared with purified 18 MΩ water. Glassware was cleaned with aqua regia and rinsed thoroughly with deionized water.

Synthesis of gold nanoparticles (AuNPs)

Citrate AuNPs (AuCIT)

AuNPs were prepared using a simple wet chemical method according to previously reported literature[25]. Briefly, 100 mL of $HAuCl_4$ (1 mM) were heated to boiling, then 6 mL of freshly prepared sodium citrate (40 mM) were added to the boiling solution quickly with strong stirring and maintained for 15–30 min. The color of the solution immediately changed from faint yellow to colorless and finally to dark purple. At the end of this process, the solution was continuously stirred until it cooled to room temperature and then kept at 4 °C.

Poly(ethylene glycol) (PEG)-AuNPs (AuPEG)

The PEG-AuNPs were prepared via displacement of citrate by thiolated Poly(ethylene glycol) (mPEG-SH) at the surface of AuNPs[26]. Briefly, 100 ml aqueous solution of citrate AuNPs were concentrated to 10 ml via centrifugation. Next, 2 ml of mPEG-SH (5000 g/mol), previously sonicated for 15 min, were added dropwise under vigorous stirring. The mixture was allowed to react for 12 h. The PEG-capped particles were purified by centrifugation at 13,500 rpm for 20 min and redispersed in water.

Synthesis of AuNPs conjugates

AuNPs were conjugated with BSA through passive adsorption, as previously described[27]. First, AuNPs were dispersed in water and diluted to different concentrations, 10–100 ppm. Then, different Au/BSA amount ratios were mixed in phosphate buffer (10 mM, PH 7.4) and incubated for 30 min and 48 h at room temperature (RT ~ 25 °C). The amount ratio between AuNPs and BSA was examined by keeping BSA constant, as shown in Table S1. Then, the mixture was split into two aliquots, one was used for direct injection, and the other was centrifuged for 10 min at 12,000 rpm (PEG-AuNPs 13500 rpm, 20 min) to remove the supernatant, and resuspended in phosphate buffer (10 mM, PH 7.4) to obtain purified AuNPs-BSA conjugates.

Evaluation of factors affecting binding equilibrium

Factors influencing the binding equilibrium of the AuNPs-BSA conjugates were fully assessed in this work. These parameters include the incubation time, pH, ionic strength of the culture medium, and Au/BSA mass ratio. To evaluate the effect of pH and ionic strength of the medium, a reference conjugate sample with an Au/BSA mass ratio of 0.6 samples was incubated in 10 mM phosphate buffer with different pH (6.0, 7.4, and 8.0). Next, samples with the same Au/BSA ratio (Au/BSA 0.6) were incubated in pH 7.4 phosphate buffer with different ionic strength (10, 20, and 30 mM). At the same time, in order to assess the effect of incubation time, the amount of AuNPs-BSA conjugates was monitored for 30 min, 1, 2, 4, 8, 16, and 24 h for all the samples analyzed. To evaluate instead the effect of the concentration of AuNPs on the binding equilibrium, various concentrations of AuNPs were mixed with BSA in different Au/BSA ratios, as shown in Table S1. Finally, all the mixture samples were injected into the AF4 system. Throughout the whole experiment, the mobile phase of the AF4 system was kept consistent with the mixing medium, which minimized the error caused by a possible continuation of the reaction during the focus step.

Gold nanoparticles concentration and size measurements

The concentration of AuNPs in the solutions was determined by UV-vis spectrum[28]. These measurements were conducted with a UV-2600i SHIMADZU UV-visible spectrophotometer (SHIMADZU, UK). To the concentration of AuNPs was estimated according to Lambert–Beer equation, Eq. (1).

$$\mathrm{A} = C \times \epsilon \times L \tag{1}$$

Where A is the absorbance, C is the molar concentration, ε is the molar extinction coefficient (molar extinction coefficients ε for individual gold nanoparticles using 2.7×10^{8} M^{-1}. CM^{-1} at 525 nm as a reference value)[29], and L is the path length (1 cm). Calculated molar concentrations were converted to ppm concentrations for subsequent calculation of amount ratios Au/BSA (the calculations of ppm concentration were carried out based on the synthesis conditions of colloidal gold, under which chloroauric acid is completely reduced)[30].

Zetasizer (Malvern Instrument Nano Series ZS, Worcestershire, UK) fitted with a red laser (633 nm) based on dynamic light scattering (DLS) and electrophoretic light scattering (ELS) was applied for measuring the size and Zeta potential of the synthesized AuNPs and the AuNPs-BSA conjugation. A disposable cell (DTS0012; Malvern Instruments, UK) was used for DLS measurements, for ELS measurements, samples were loaded into a clear zeta cell (DTS1070; Malvern Instruments, UK). The experimental parameters are as follows: measurements angle 173°, temperature 25 °C, and each sample was collected at least three times. The data were collected and analyzed with Malvern Software ver. 7.13.

AF4 multidetector platform setup

The AF4 system used is an AF2000 Multiflow asymmetrical flow field flow fractionation system manufactured by Postnova Analytics (Germany) which contains a Postnova PN7520 solvent degasser, two Postnova PN1130 Isocratic Pumps was used to solvent delivery and a special cross-flow control, using a unique dual syringe pump module with non-pulsing crossflow delivery for most precise separation conditions. All the samples were separated in a trapezoidal separation channel with 350 µm thick (thickness of the spacer), which equipped with a regenerated cellulose membrane with 10 kDa cutoff as accumulation wall. The system is followed by a PN3242 4-channel UV-Vis/DAD detector and a 21-angle multiangle light scattering detector, MALS (PN3621). NovaFFF version 2.2.0.1 software was used to control the instruments, set separation parameters, collect data, handle signals from the detectors (MALS and DAD), and compute the radius and molar mass of particles during measurements. MALS molar mass and size relative calibrations were performed using a software incorporated with the instrument (NovaFFF version 2.2.0.1) trough BSA injections, which allowed us to monitor the conformation state of each population[31].

Method optimization has extensively been described in a previous work[22]. All samples were tested using the following AF4 method. Firstly, the samples were loaded in the system at a rate of 0.2 mL/min. During the injection step, 3 min focusing time was used at a rate of 3.3 mL/min with a cross-flow set at 3 mL/min. After a transition period of 0.2 min, the cross flow was kept at 3 mL/min for 6 min. And then, the cross flow decreased with an exponent decay of 3 mL/min to 0.4 mL/min within 10 min, and finally down to 0 mL/min from 0.4 mL/min with a linear rate within 15 min. The detector flow was always kept along the process constant at 0.5 mL/min to obtain a stable baseline. To make all the species elute out from the channel, a 5 min rinse step was conducted at each injection. Two characteristic wavelengths were set at 280 nm for protein and 525 nm for gold and the corresponding signals were collected.

Results

Batch characterization of AuNPs and AuNPs conjugates

Spherical AuNPs are characterized by surface plasmon resonance (SPR), with a visible peak between 520 and 580 nm for particle ranging from 2.5 to 100 nm[32]. Alterations in AuNPs shape, size, and nature can be detected by monitoring the shift of the absorbance maximum of the SPR band. The UV/Vis absorption spectra of AuCIT and PEG-AuNPs displayed a SPR band at 525 nm and both of them moved to higher wavelength in the presence of BSA (Fig. 1).

The absorption spectra change as a result of protein binding to AuNPs has been widely reported[33]. In addition, when increasing the starting concentration of AuNPs in the mixture, the absorbance intensity at 278 nm increased (Fig. 2A,B)[34]. This optical feature has been observed both for Citrate and PEG-AuNPs measurements and can be associated to the absorption of BSA onto AuNPs' surface generating bioconjugates[35]. On the other hand, the data obtained from the Zeta potential measurements show that AuCIT were characterized by a lower

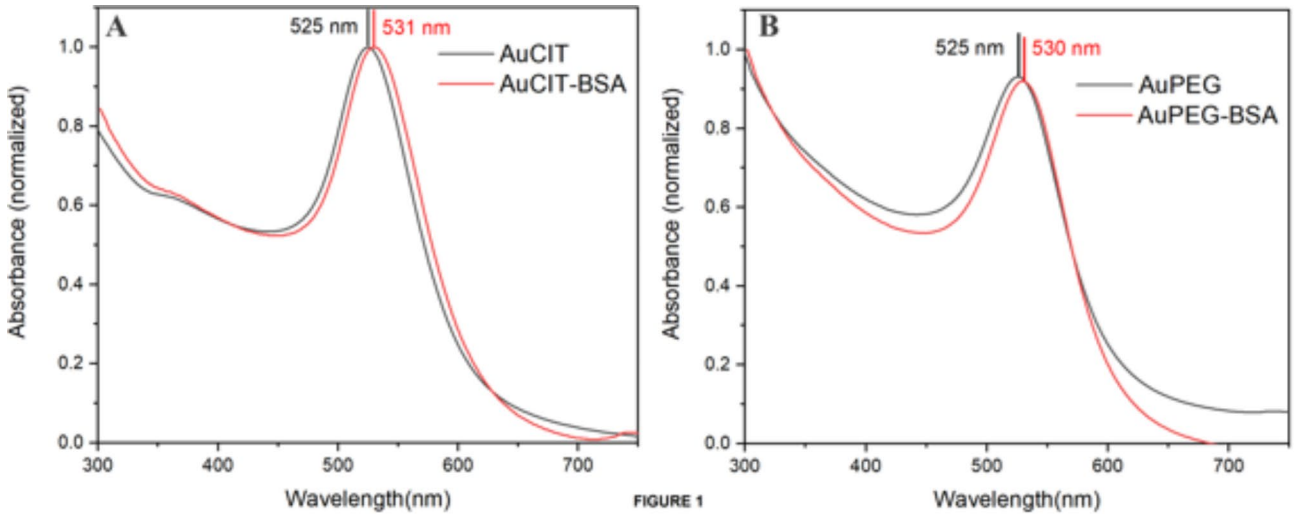

Fig. 1. UV-Vis absorbance spectra of (**A**) AuCIT and AuCIT-BSA mixture (**B**) AuPEG and AuPEG-BSA mixture obtained from UV spectrophotometer (all spectra were normalized to the maximum absorbance peak intensity of AuCIT at 525 nm).

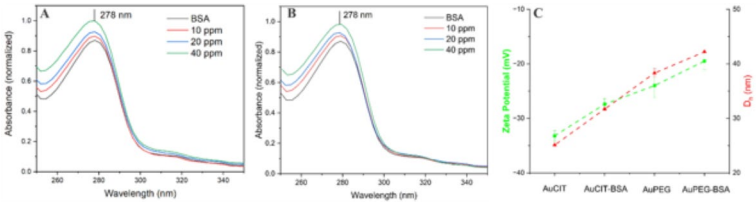

Fig. 2. UV-Vis absorbance spectra of BSA (100 ppm) and after 1 h incubation with different concentrations of AuCIT (**A**) and AuPEG (**B**) (10 ppm, 20 ppm, 40 ppm) (all spectra were normalized to the absorbance intensity of AuCIT 40 ppm at 278 nm). (**C**) Z-Potential and hydrodynamic diameter measurements of AuNPs and their conjugates (all samples were dispersed in phosphate buffer, pH 7.4).

Z-potential compared to PEG-AuNPs while BSA adsorption caused a partial neutralization for both AuNPs (Fig. 2C). Moreover, the size information of freshly synthesized AuNPs and the mixture samples after 30 min incubation with BSA from dynamic light scattering (DLS) (shown in Table S2) also indicated that BSA was successfully bound to AuNPs.

However, it is difficult to obtain the stoichiometry information of AuNPs-BSA conjugates with this data due to the intrinsic limitation of batch techniques (DLS and UV/vis) preventing exploring the binding behavior of the reaction unit in a mixture medium[36]. Therefore, an AF4-multidetection platform was introduced to further characterize the mixture samples by the means of spectroscopy and laser scattering while efficiently separating the mixture samples based on their hydrodynamic size.

Assessment of AF4 Method robustness

Before systematically screening synthetic bioconjugates under various parameter conditions, it is crucial to ensure that both the system and the developed method consistently yield reproducible results. This is essential for accurately monitoring any fractograms change caused by the samples during the testing process.

Therefore, we verified reproducibility along different weeks of testing, using standard batches of AuCIT and AuPEG in water, which have a stable radius confirmed via dynamic light scattering (DLS) (Table S2). As shown in Fig. 3A,D, both AuNPs showed excellent reproducibility in different weeks (Relative Standard Deviation (RSD) of the intensity 1.95% for AuCIT and 1.45% for AuPEG). Simultaneously, a standard concentration of BSA (100 ppm) dispersed in phosphate buffer was also used to verify the stability of the entire instrument system and method robustness (Fig. 3B,E, green). Furthermore, the conjugation was performed by mixing AuNPs and BSA with an Au/BSA mass ratio of 0.6 and 1 h incubation prior to injection (Fig. 3B,E, red) under the stable-most conditions. In 4 weeks of analysis repetitions, all analyses howed high reproducibility and stability, whether it was standard AuNPs or bioconjugates synthesized under the most stable conditions. Based on the peak position and shape, we can conclude that during this period, the instrument system and method remained consistent, with no uncontrollable variables affecting the experimental results. Therefore, any changes observed in the chromatography when systematically screening synthetic bioconjugates under various parameter conditions should be attributed to the samples.

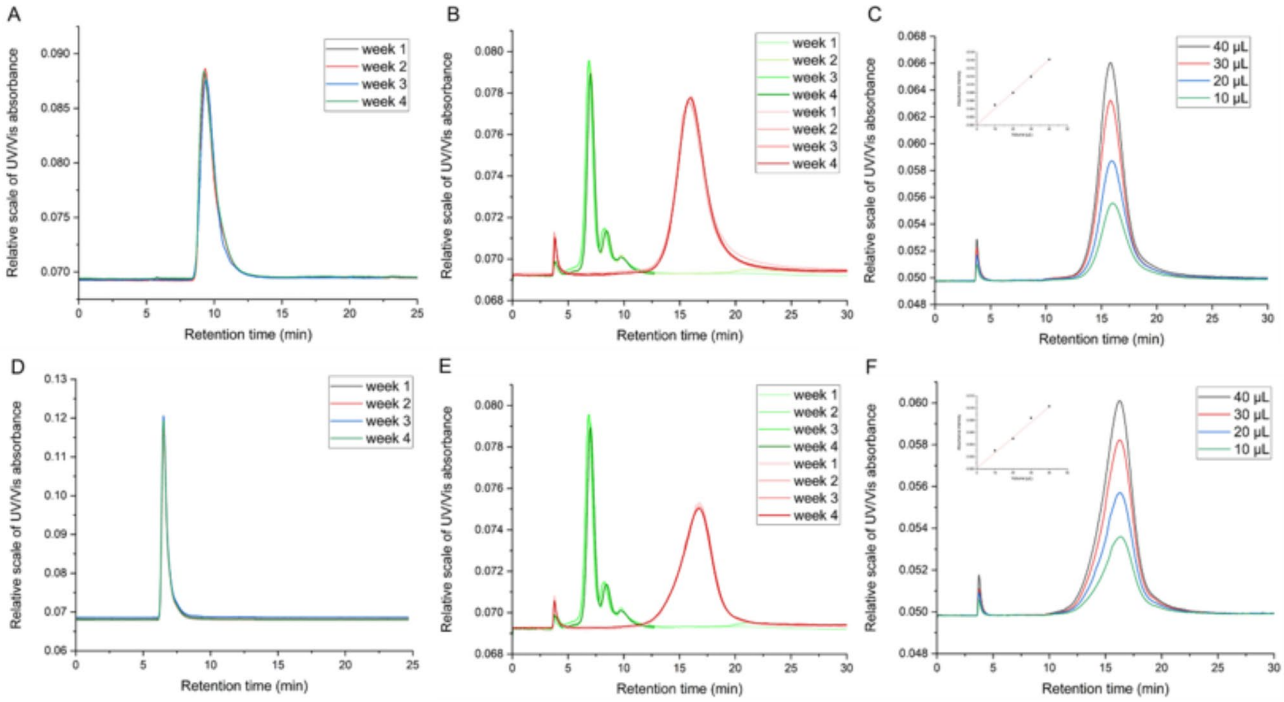

Fig. 3. AF4-UV/Vis fractograms (525 nm) of fresh AuCIT (**A**) and AuPEG (D). (**B**) AF4-UV/Vis fractograms of standard BSA (20 µg) (280 nm, green) and AuCIT-BSA (525 nm, red) in phosphate buffer. (**C**) AF4-UV/Vis fractograms of (525 nm) fresh AuCIT-BSA with different injection volumes in phosphate buffer (insert: linearity as injection volume vs. intensity). (**E**) Overlay of AF4-UV/Vis fractograms of standard BSA (20 µg) (280 nm, green) and AuPEG-BSA (525 nm, red) in phosphate buffer. (**F**) AF4-UV/Vis fractograms of (525 nm) fresh AuPEG-BSA with different injection volumes in phosphate buffer (insert: linearity as injection volume vs. intensity).

In addition, linearity was checked to verify the operational range and the influence of injection volume, as shown in Fig. 3C,F. With the increase in injection volume, the peak shape and peak position of the two conjugates did not change, and the absorbance intensity exhibited an expected linear increment,(shown as injection volume vs. intensity in Fig. 3C,F (insets)).

Analyzing the above experimental results from a methodological perspective, we can conclude that we have developed a robust AF4 method. This method not only effectively separates individual standard samples but also demonstrates excellent separation capabilities for complex mixed samples. Therefore, we can reliably monitor various stages of the synthesis process, such as different reaction times, reactant ratios, and reaction environments.

Size characterization of AuNPs Conjugates

The measurements were conducted following a 1 h incubation period (as we verified that the peak reached plateau), with subsequent evaluations performed after 48 h to monitor for any alterations over time. After 48 h, no changes in retention time or signal intensity were observed in the chromatograms of AuPEG-BSA, while a minor time shift of less than 1% was detected in the chromatograms of Citrate AuNPs-BSA conjugates following the 48 h incubation period. The AF4-UV/Vis fractograms were shown in Fig. S1 and the size expressed as gyration radius (Rg) was plotted and overlaid with fractograms. MALS results highlighted the presence of two populations (P1 and P2) for both conjugates at different time, and the corresponding size characterization results are reported in Table 1.

Firstly, P1 is fairly monodisperse for both conjugates after 1 h and represents the majority of the sample content since the P1/P2 area ratio is around 20:1. However, after 48 h, the AuPEG-BSA conjugates showed a loss of monodispersity (PdI 1.132) and size decreases in P1, which may be caused by the insufficient binding between PEG and BSA,reflecting a higher instability to conjugation than bare AuCIT. The shape factor, expressed as the ratio between gyration and hydrodynamical radius, would equal to 0.653 and 0.610 for the AuCIT-BSA conjugates and AuPEG-BSA conjugates respectively (Data for Rh is presented in the supplementary information). A value of 0.77 is expected for a compact sphere while a shape factor of 0.6/0.5 is typical for core-shell systems[37]. The P2's particles are quite stable, account for only 5% of the total signal and can be removed from the conjugates by means of fractionation, which has a great impact on the signal response of the sensor and the quantitative study based on the protein targets.

	Rg (nm)		Rg (average, nm)	PdI	Shape factors (Rg/Rh)
	P1	P2			
AuCIT-BSA-30 min	8.9	11–30	10.4	1.002	0.653
AuCIT-BSA-48 h	8.7	10–34	11.4	1.010	0.708
AuPEG-BSA-30 min	9.5	11–34	12.8	1.020	0.610
AuPEG-BSA-48 h	7.7	6.5–35	13.3	1.132	0.630

Table 1. The size information form MALS (gyration radius, rg; hydrodynamic radius, Rh. PdI of a monodisperse sample = 1.000).

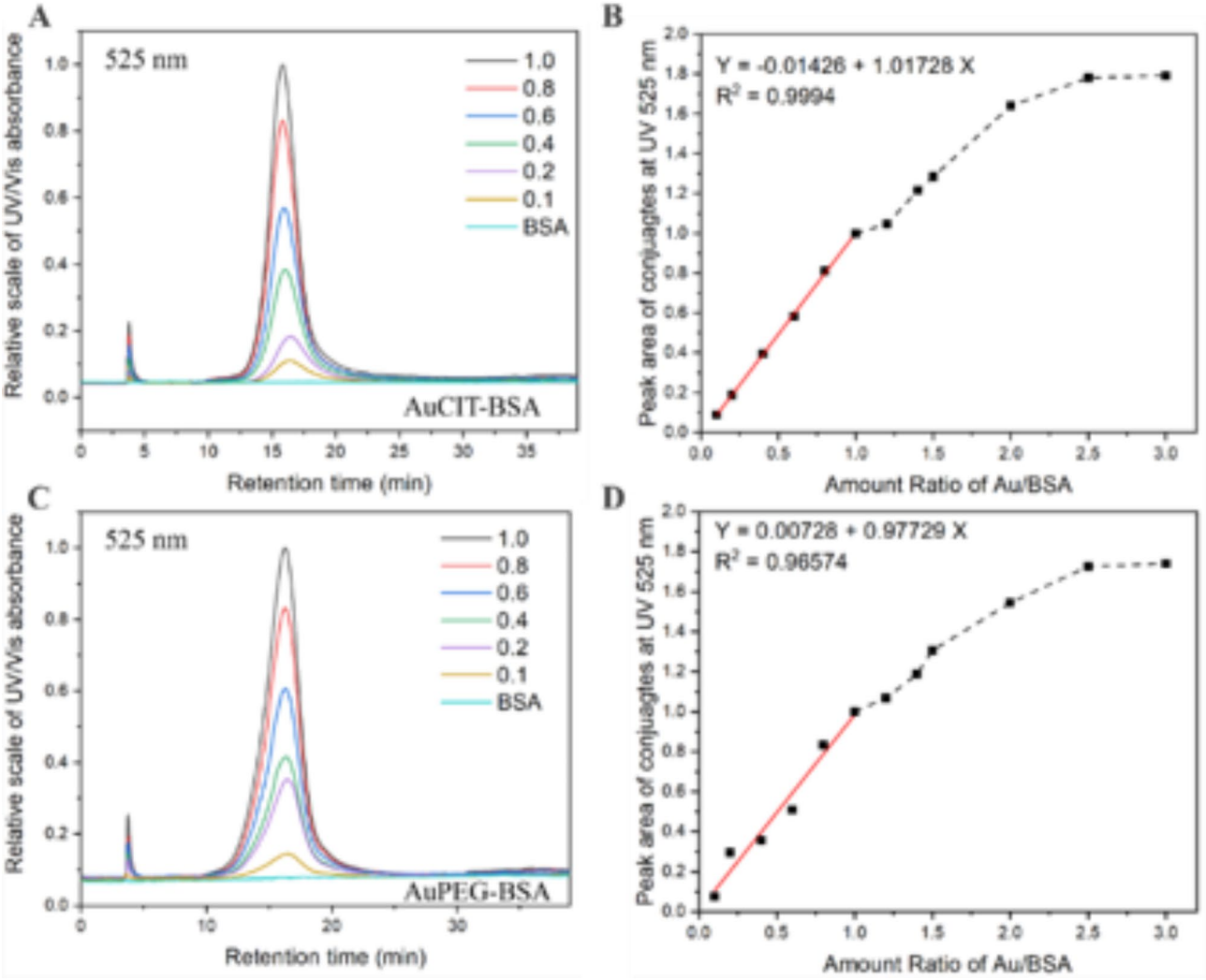

Fig. 4. AF4 coupling with UV/Vis absorbance signal for different Au/BSA amount ratios 0.1, 0.2, 0.4, 0.6, 0.8, and 1.0 (keep amount of BSA constant). (**A**) AF4-UV/Vis fractograms of AuCIT-BSA conjugates at 525 nm. (**B**) The peak area of AuCIT-BSA conjugates at 525 nm as a function of amount ratio of Au/BSA. (**C**) AF4-UV/Vis fractograms of AuPEG-BSA conjugates at 525 nm. (**D**) The peak area of AuPEG-BSA conjugates at 525 nm as a function of amount ratio of Au/BSA. (solid line: Au/BSA ratio 0.1-1, dotted line: Au/BSA ratio1.2-3.0)

Effect of AuNPs and BSA ratio on AuNPs conjugates

Concentration is often the most important factor affecting the formation of conjugates due to the existence of competitive reactions and steric hindrance effects[38]. To estimate the impact of AuNPs concentration on the binding behavior, increasing concentrations of AuNPs from 10 to 100 ppm were incubated with the same amount of BSA. As shown in Fig. 4A and C, the AF4 absorbance fractograms at 525 nm increases gradually

with increasing the amount of gold while maintaining the same BSA excess, suggesting that more AuNPs have combined with BSA to form conjugates.

The conjugates area as a function of reactant ratio were plotted in Fig. 4B,D, where both conjugates show a linear increasing trend (R^2 0.9994 and R^2 0.96574 for AuCIT-BSA and AuPEG-BSA conjugates, respectively) in a specific range of Au/BSA ratio (i.e. within 0.1 and 1). Moreover, it's worth noticing that the shape and trend of the fractogram did not change with the changing in Au/BSA ratio for either AuCIT or AuPEG demonstrating that Au/BSA reactant ratios equal or lower than 1 didn't impact the binding behavior. Considering linear fitting and fractogram reproducibility, both conjugates demonstrate remarkable stability (Au/BSA ratio 0.1-1.0), with AuCIT exhibiting superior conjugation performance.

Interestingly, as we keep increasing the amount ratio of AuNPs (Au/BSA ratio1.2-3.0), the amount of both conjugates is gradually increasing, while its growth rate gradually decreases, as shown in the black dashed lines of Fig. 4B,D. The competitive reaction caused by the existence of a large number of AuNPs and the aggregation caused by too high local concentration are the main reasons why the amount of conjugates cannot continue to maintain a linear growth rate and stability. No additional conjugates formation is observed for Au/BSA ratios higher than 2.5. Noteworthy, the shape of the fractograms of AuNPs-BSA conjugates from Au/BSA ratio1.2-2.5 at 525 nm is the same as Au/BSA ratio 0.1-1, as shown in Fig. S2, suggesting that the excessive AuNPs did not affect their binding behavior. Optimal conjugation efficiency and stability can be achieved under the conditions of amount ratio 1:1, while increasing the nanoparticle ratio to 2.5-3.0 is required to maximize the conjugates product. In the subsequent screening of conjugates across multiple environments and parameters, a stable and representative Au/BSA ratio of 0.6 was selected.

Stability of AuNPs conjugates

Both conjugates (1 h and 48 h) of Citrate and PEG AuNPs were subjected to a centrifugation to remove the excess BSA. After centrifugation the precipitated pellets (conjugates) were separated from the supernatant (containing BSA) and resuspended in mobile phase. The resulting samples were then injected immediately (CEN) or after 48 h (CEN-48 h) into the AF4 system.

For both mixture samples, the BSA characteristic peak disappeared in the fractogram at 280 nm after centrifugation, which confirms that the AuNPs-BSA conjugates, as expected, can also be enriched by centrifugation (Figure S3). However, the conjugated sample is also partially lost during centrifugation, corresponding to a decrease in the absorbance intensity and area of the conjugates peak. For example, as shown in Fig. 5, after the centrifuged sample was left for 48 h, AuCIT-BSA conjugates exhibited a signal attenuation of 17.8% (both at 280 nm and 525 nm), and the AuPEG-BSA conjugates showed a signal attenuation of nearly 60%, suggesting differential adsorption stability regarding AuCIT or AuPEG and BSA conjugation.

AF4 analysis of uncentrifuged conjugates showed instead unvaried recovery and no decrease over time: as a soft separation technique it allows rapid separation of ready-to-use conjugates with minimal sample loss. The negative impact of centrifugation also provides a different perspective on the stability of BSA conjugates. In fact, when we further characterized the samples that have been left for 48 h after centrifugation (1 h CEN 48 h), we observed an even higher sample loss than that of the freshly centrifugated sample (1 h/48 h CEN), especially for what concerns AuPEG conjugates. This intriguing phenomenon gives us a deeper insight into the role of BSA in conjugates formation and stability, suggesting that the presence of BSA can promote and stabilize bioconjugate formation on AuNPs surface[39].

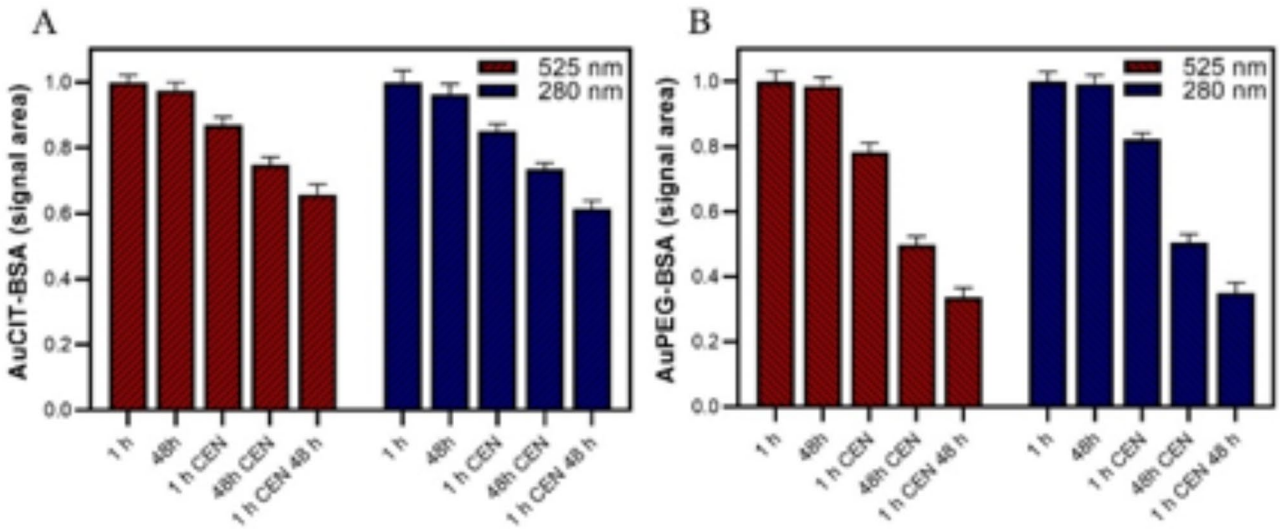

Fig. 5. Area values of conjugates (Au – BSA ratio = 0.6) at 525 and 280 nm, normalized to the absorbance of AuCIT-BSA (**A**) and AuPEG-BSA (**B**) conjugates at 1 h. AuCIT-BSA and AuPEG-BSA mixtures were incubated and then injected or centrifuged (CEN) and then injected. After 1 h of incubation, an aliquot was also centrifuged and left to stand for 48 h (MIX 1 h CEN-48 h).

Screening of AuNPs conjugates under various environments and parameters

Though the binding equilibrium is basically established after 1 h in phosphate buffer (10 mM, pH 7.4), the binding equilibrium is affected by many factors[40]. Thus, pH and ionic strength were studied to examine how they impact the surface properties of the nanoparticles and the binding behavior of the protein and an additional timepoint was added at 30 min from the incubation start to better visualize different trends.

In the physiological environment, the pH value will change under certain pathological conditions, such as in the tumor microenvironment, where the pH value is usually lower than the normal physiological level (close to pH 6.5-7.0). In some metabolically active intracellular environments, the pH value may increase[41]. Therefore, the selection of pH 6.0–8.0 can help us evaluate the stability of AuNPs-BSA conjugates under normal or non-normal physiological conditions. To explore the effect of pH, the mixtures were incubated in 10 mM phosphate buffer with different pH levels (6.0, 7.4, and 8.0) and then injected into AF4 system without pre-purification. For the AuCIT-BSA mixture samples, the binding equilibrium showed a lagged trend from 30 min to 4 h under acidic and alkaline culture conditions, which means that the change of pH makes the adsorption of BSA to the surface of AuNPs more difficult, as shown in Fig. 6A. Especially under alkaline conditions, this process is significantly suppressed resulting in a significant drop in the amount of conjugate formed.

On the contrary, for AuPEG, the change in the density of surface charge caused by pH can be effectively avoided due to the protection of PEG. On the other hand, the absorption intensity of AuPEG-BSA is still highest at physiological pH, indicating that the electrical properties of BSA were also affected by it. Furthermore, it should be noted that the reduction in the conjugate signal was not caused by the aggregation of the AuNPs in the culture medium, since the conjugates' peak does not shift with longer incubation time, and no impurities are eluted from the channel during the monitoring process (data shown in Fig. S4A,C). Unreacted AuCIT are instead destabilized during the focusing phase of AF4 and attached to the membrane, as we analyzed in detail in our previous study. Therefore, the change in pH has a great influence on the binding equilibrium site, while the stability of the formed conjugates was not affected, which is also consistent with the results showing that the presence of excess BSA can promote the stability of the conjugates.

To further explore the effect of ionic strength on this process, the mixture samples were incubated in pH 7.4 phosphate buffer with different ionic strength levels (10, 20, and 30 mM). During the synthesis of conjugates, high

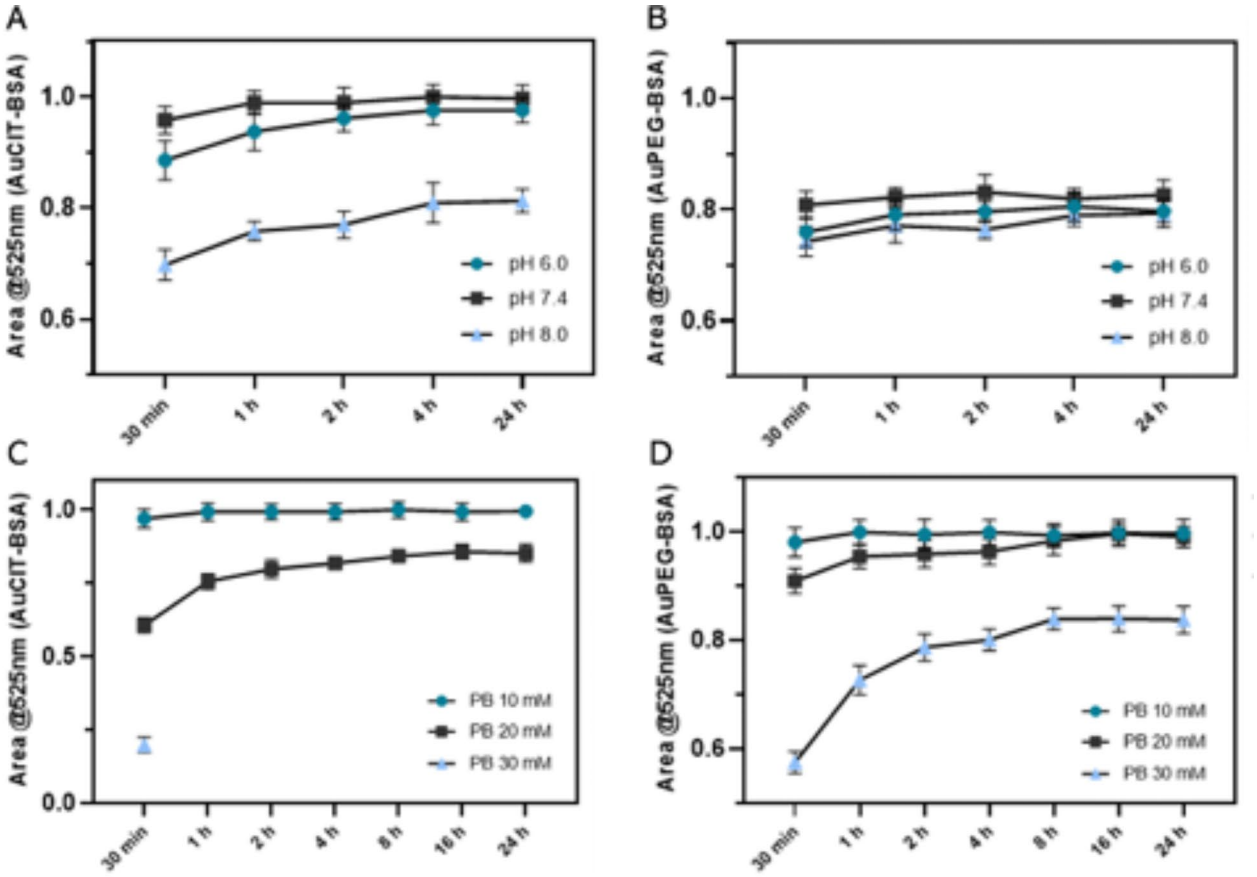

Fig. 6. The normalized peak area of conjugates at 525 nm as a function of incubation time (normalized to the peak area of AuCIT/PEG-BSA conjugates at 1 h, PB 10 mM pH 7.4). (**A**,**B**) AuCIT-BSA mixture and AuPEG-BSA mixture incubated in phosphate buffer (10 mM) at different pH 6.0, 7.4, and 8.0. (**C**,**D**) AuCIT-BSA mixture and AuPEG-BSA mixture incubated in phosphate buffer (pH 7.4) at different concentrations 10, 20, and 30 mM.

ionic strength reaction solutions are generally avoided to maintain nanoparticle stability. If high ionic strength is required, it is usually to simulate dilute bodily fluids or biological separation media, which have relatively low ionic strength. For example, cell culture medium (diluted): 5–30 mM, used for cell biology experiments and studies of the interaction of nanoparticles in the extracellular environment[42]. In order to minimize the error generated by the system, the mobile phase of the AF4 system is consistent with the medium. Characterization of the incubation time showed that the conjugates of both samples could rapidly reach the binding equilibrium site under the condition of 10 mM, as shown in Fig. 6C and D. Furthermore, at 10 mM, the area of the conjugate peaks for both mixtures incubated for 30 min were much higher than those at 20 and 30 mM, suggesting that ionic strength largely hinders the binding between the reactive units. In this respect, Electrostatic interaction becomes the main interaction force between gold nanoparticles and BSA under natural conditions. Meanwhile, as the ionic strength increased, the conjugates' intensity and retention time of the both samples changed, especially in the 30 mM medium (data shown in Fig. S4B,D).

For the AuCIT-BSA mixture, the conjugates peak did not undergo a large shift in the 20 mM medium, but the absorption intensity decreased, and binding equilibrium time moved to 16 h compared to the samples in the 10 mM medium. Notably, a large number of impurities eluted out from the channel at the end of the measurements, suggesting the aggregation of AuNPs during the incubation in the 20 mM medium. However, we did not find a shift of the conjugates peak, which means that the conjugates though unstable can partially co-exist at least under 20 mM medium. As we continued to increase the concentration of the medium, the peak of the conjugates moved to 20 min generating a wide band-like signal spreading till the end of the measurement. These observations suggest that not only the AuNPs aggregated but the conjugates protected by the protein aggregated as well as the concentration of the buffer solution increased. To avoid further fouling on the membrane, we did not monitor other time points in a 30 mM medium.

Compared with AuCIT, even at 20 mM medium, AuPEG-BSA conjugates can eventually reach the same intensity/area as at 10 mM medium, as shown in Fig. 6D. Therefore, AuPEG have relatively higher stability in the same medium and the establishment of binding equilibrium sites is possible and faster than that if AuCIT (8 h versus 16 h). In 30 mM medium, the AuPEG-BSA conjugates exhibited the same degree of shift as the AuCIT-BSA conjugates. The difference is the presence of a distinct conjugates peak in the profile of the AuPEG-BSA mixture, which tends to be stable in the follow-up monitoring. However, we found that the fractogram could not drop to the baseline range until the end of the measurement during the 25–35 min interval and the intensity gradually increases over incubation time. As the number of injections increases impurities will gradually accumulate on the membrane surface, as shown in Fig. S5.

Overall, by combining the results obtained, we found that while AuNPs with PEG coating exhibit greater stability at high salinities, such as 30 mM (Fig. 6), their conjugates are less stable over time and shift during elution (Fig. 5 and S5). In contrast, although bare AuCIT are significantly affected by pH and salt concentration, once conjugates are formed, their time and purification stability surpasses that of the conjugates formed with AuPEG. The approach of scanning different mixture ratios, exploring stability over time and in different saline media proved as an efficient way to obtain relevant information in a short time and with a low amount of sample, streamlining the selection of optimal parameters or optimal starting materials for the application envisaged.

Conclusion

In summary, we designed an analytical method based on asymmetric flow field flow fractionation (AF4) with photodiode array and multiangle light scattering detector (AF4-DAD-MALS) to study and screen the bioconjugates in application media. AuNPs protected by two types of surface coating (PEG and Citrate) were used as main research subjects to produce bioconjugates with BSA to form bioconjugates under various conditions, such as different reactant ratios and different solution environments. Firstly, the developed method allows for a rapid and soft purification and collection of the analytes without effecting their nature, which shows a wide size range (Rh up to 80 nm) and a range of proteins and ligands with molecular weights ranging from 10 to 200 kDa. Next, further attention was put in investigating the influence of Au/BSA mass ratios, which allowed to identify the yield-maximizing (1:1) and product-maximizing (2.5:1) conditions for the generation of AuNPs-protein conjugates. During the purification and screening stages, AuPEG shows higher stability in solution due to the steric hindrance effect brought by PEG, but exhibits low conjugation tendency and conjugates stability compared to AuCIT. In addition, we found that changes in salt concentration tended to affect bare AuCIT particles, while changes in pH had a more dramatic effect on AuPEG. These studies are carefully designed to reflect the application environment, be non-destructive, possibly provide more information with one analysis, identify different co-existing species, and provide fast results to enable prompt screenings of many different conjugates at a time. Therefore, we can adjust the synthesis conditions according to the requirements of different samples in future applications, and predict and simulate multiple combinations at low amounts of samples.

Data availability

Data is provided within the manuscript and supplementary information files. Additional information and raw data can be made available upon reasonable request by contacting the corresponding author.

Received: 14 June 2024; Accepted: 19 September 2024
Published online: 30 December 2024

References

1. Abdel-Mageed, H. M., AbuelEzz, N. Z., Radwan, R. A. & Mohamed, S. A. Nanoparticles in nanomedicine: A comprehensive updated review on current status, challenges and emerging opportunities. *J. Microencapsul.* **38** (6), 414–436. https://doi.org/10.1080/02652048.2021.1942275 (2021).
2. Wang, L. et al. The density of Surface Coating can contribute to different antibacterial activities of gold nanoparticles. *Nano Lett.* **20** (7), 5036–5042. https://doi.org/10.1021/acs.nanolett.0c01196 (2020).
3. Delong, R. K. et al. Functionalized gold nanoparticles for the binding, stabilization, and delivery of therapeutic DNA, RNA, and other biological macromolecules. *Nanotechnol Sci. Appl.* **3**, 53–63. https://doi.org/10.2147/nsa.S8984 (2010). From NLM.
4. Khaniani, Y. et al. A gold nanoparticle-protein G electrochemical affinity biosensor for the detection of SARS-CoV-2 antibodies: A surface modification approach. *Sci. Rep.* **12** (1), 12850. https://doi.org/10.1038/s41598-022-17219-7 (2022).
5. Chirra, H. D., Sexton, T., Biswal, D., Hersh, L. B. & Hilt, J. Z. Catalase-coupled gold nanoparticles: Comparison between the carbodiimide and biotin–streptavidin methods. *Acta Biomater.* **7** (7), 2865–2872. https://doi.org/10.1016/j.actbio.2011.01.003 (2011).
6. Smith, J. E. et al. Colorimetric detection with aptamer-gold nanoparticle conjugates coupled to an android-based color analysis application for use in the field. *Talanta*. **121**, 247–255. https://doi.org/10.1016/j.talanta.2013.12.062 (2014).
7. Germain, M. et al. Delivering the power of nanomedicine to patients today. *J. Controlled Release*. **326**, 164–171. https://doi.org/10.1016/j.jconrel.2020.07.007 (2020).
8. Li, L., Mu, Q., Zhang, B. & Yan, B. Analytical strategies for detecting nanoparticle–protein interactions. *Analyst*. **135** (7), 1519–1530. https://doi.org/10.1039/C0AN00075B (2010).
9. Mariam, J., Dongre, P. M. & Kothari, D. C. Study of Interaction of Silver nanoparticles with bovine serum albumin using fluorescence spectroscopy. *J. Fluoresc*. **21** (6), 2193. https://doi.org/10.1007/s10895-011-0922-3 (2011).
10. Dobrovolskaia, M. A. et al. Interaction of colloidal gold nanoparticles with human blood: effects on particle size and analysis of plasma protein binding profiles. *Nanomed. Nanotechnol Biol. Med.* **5** (2), 106–117. https://doi.org/10.1016/j.nano.2008.08.001 (2009).
11. Deng, Z. J. et al. Differential plasma protein binding to metal oxide nanoparticles. *Nanotechnology*. **20** (45), 455101. https://doi.org/10.1088/0957-4484/20/45/455101 (2009).
12. Lundqvist, M. et al. Nanoparticle size and surface properties determine the protein corona with possible implications for biological impacts. *Proc. Natl. Acad. Sci.* **105**(38), 14265–14270. https://doi.org/10.1073/pnas.0805135105 (2008).
13. Boulos, S. P. et al. Nanoparticle–protein interactions: a thermodynamic and kinetic study of the adsorption of bovine serum albumin to Gold Nanoparticle surfaces. *Langmuir*. **29** (48), 14984–14996. https://doi.org/10.1021/la402920f (2013).
14. Treuel, L., Malissek, M., Gebauer, J. S. & Zellner, R. The influence of Surface Composition of nanoparticles on their interactions with serum albumin. *ChemPhysChem*. **11** (14), 3093–3099. https://doi.org/10.1002/cphc.201000174 (2010). (acccessed 2022/12/21).
15. Zappi, A. et al. Extracting information and enhancing the quality of separation data: A review on Chemometrics-assisted analysis of Volatile, Soluble and Colloidal Samples. *Chemosensors*. **11** (1), 45. https://doi.org/10.3390/chemosensors11010045 (2023).
16. Marassi, V. et al. Synthesis monitoring, characterization and cleanup of Ag-Polydopamine nanoparticles used as Antibacterial agents with Field-Flow Fractionation. *Antibiotics*. **11** (3). https://doi.org/10.3390/antibiotics11030358 (2022).
17. Leeman, M. et al. Asymmetric flow field-flow fractionation coupled to surface plasmon resonance detection for analysis of therapeutic proteins in blood serum. *Anal. Bioanal Chem.* **413** (1), 117–127. https://doi.org/10.1007/s00216-020-03011-x (2021).
18. Qureshi, R. N. & Kok, W. T. Application of flow field-flow fractionation for the characterization of macromolecules of biological interest: a review. *Anal. Bioanal. Chem.* **399** (4), 1401–1401. https://doi.org/10.1007/S00216-010-4278-3 (2011).
19. Marassi, V. et al. FFF-based high-throughput sequence shortlisting to support the development of aptamer-based analytical strategies. *Anal. Bioanal Chem.* **414** (18), 5519–5527. https://doi.org/10.1007/s00216-022-03971-2 (2022).
20. Marassi, V., Giordani, S., Reschiglian, P., Roda, B. & Zattoni, A. Tracking heme-protein interactions in healthy and pathological human serum in native conditions by miniaturized FFF-Multidetection. *Appl. Sci.* **12** (13). https://doi.org/10.3390/app12136762 (2022).
21. Ventouri, I. K., Loeber, S., Somsen, G. W., Schoenmakers, P. J. & Astefanei, A. Field-flow fractionation for molecular-interaction studies of labile and complex systems: A critical review. *Anal. Chim. Acta*. **1193**, 339396–339396. https://doi.org/10.1016/J.ACA.2021.339396 (2022).
22. Wang, J. et al. Quality control and purification of ready-to-use conjugated gold nanoparticles to ensure effectiveness in biosensing. *Front. Sens.***3**https://doi.org/10.3389/fsens.2022.1087115 (2022). Original Research.
23. Mirón-Mérida, V. A. et al. Aptamer–Target–Gold Nanoparticle conjugates for the quantification of fumonisin B1. *Biosensors* **11** (1), 18. (2021).
24. Bouzas-Ramos, D., García-Alonso, J. I., Costa-Fernández, J. M. & Ruiz Encinar, J. Quantitative Assessment of Individual Populations Present in nanoparticle–antibody Conjugate mixtures using AF4-ICP-MS/MS. *Anal. Chem.* **91** (5), 3567–3574. https://doi.org/10.1021/acs.analchem.8b05482 (2019).
25. Wang, J. et al. Recyclable and ultrasensitive SERS sensing platform: deposition of atomically precise Ag152 nanoclusters on surface of plasmonic 3D ZnO-NC/AuNP arrays. *Appl. Surf. Sci.* **540**, 148324. https://doi.org/10.1016/j.apsusc.2020.148324 (2021).
26. Fernández-López, C. et al. Highly controlled silica coating of PEG-Capped Metal nanoparticles and Preparation of SERS-Encoded particles. *Langmuir*. **25** (24), 13894–13899. https://doi.org/10.1021/la9016454 (2009).
27. Safenkova, I. V., Zherdev, A. V. & Dzantiev, B. B. Correlation between the composition of multivalent antibody conjugates with colloidal gold nanoparticles and their affinity. *J. Immunol. Methods*. **357** (1), 17–25. https://doi.org/10.1016/j.jim.2010.03.010 (2010).
28. Haiss, W., Thanh, N. T. K., Aveyard, J. & Fernig, D. G. Determination of size and concentration of gold nanoparticles from UV – vis Spectra. *Anal. Chem.* **79** (11), 4215–4221. https://doi.org/10.1021/ac0702084 (2007).
29. Dolinnyi, A. I. Extinction coefficients of gold nanoparticles and their dimers. Dependence of optical factor on particle size. *Colloid J.* **79** (5), 611–620. https://doi.org/10.1134/S1061933X17050052 (2017).
30. Campos, A. R. et al. Quantifying gold nanoparticle concentration in a Dietary supplement using Smartphone Colorimetry and Google Applications. *J. Chem. Educ.* **93** (2), 318–321. https://doi.org/10.1021/acs.jchemed.5b00385 (2016).
31. Marassi, V. et al. Perspectives on protein biopolymers: miniaturized flow field-flow fractionation-assisted characterization of a single-cysteine mutated phaseolin expressed in transplastomic tobacco plants. *J. Chromatogr. A*. **1637**, 461806. https://doi.org/10.1016/j.chroma.2020.461806 (2021).
32. Dong, Y. C. et al. Effect of gold nanoparticle size on their properties as contrast agents for computed tomography. *Sci. Rep.* **9** (1), 14912. https://doi.org/10.1038/s41598-019-50332-8 (2019).
33. Liu, F. et al. Modulating the activity of protein conjugated to Gold nanoparticles by Site-Directed Orientation and Surface density of bound protein. *Acs Appl. Mater. Inter.* **7** (6), 3717–3724. https://doi.org/10.1021/am5084545 (2015).
34. Wimuktiwan, P., Shiowatana, J. & Siripinyanond, A. Investigation of silver nanoparticles and plasma protein association using flow field-flow fractionation coupled with inductively coupled plasma mass spectrometry (FlFFF-ICP-MS). *J. Anal. Spectrom.* **30** (1), 245–253. https://doi.org/10.1039/C4JA00225C (2015).
35. López-Sanz, S., Fariñas, N. R., Martín-Doimeadios, R. C. R. & Ríos, Á. Analytical strategy based on asymmetric flow field flow fractionation hyphenated to ICP-MS and complementary techniques to study gold nanoparticles transformations in cell culture medium. *Anal. Chim. Acta*. **1053**, 178–185. https://doi.org/10.1016/j.aca.2018.11.053 (2019).

36. Bell, N. C., Minelli, C. & Shard, A. G. Quantitation of IgG protein adsorption to gold nanoparticles using particle size measurement. *Anal. Methods*. **5** (18), 4591–4601. https://doi.org/10.1039/C3AY40771C (2013).
37. Marassi, V. et al. Silver nanoparticles as a medical device in healthcare settings: A five-step approach for candidate screening of coating agents. *R. Soc. Open. Sci.* **5** (1), 171113. https://doi.org/10.1098/rsos.171113 (2018).
38. Ostermeyer, A. K., Kostigen Mumuper, C., Semprini, L. & Radniecki, T. Influence of bovine serum albumin and Alginate on Silver Nanoparticle dissolution and toxicity to Nitrosomonas europaea. *Environ. Sci. Technol.* **47** (24), 14403–14410. https://doi.org/10.1021/es4033106 (2013).
39. Sermsri, W., Jarujamrus, P., Shiowatana, J. & Siripinyanond, A. Flow field-flow fractionation: A versatile approach for size characterization of α-tocopherol-induced enlargement of gold nanoparticles. *Anal. Bioanal Chem.* **396** (8), 3079–3085. https://doi.org/10.1007/s00216-010-3511-4 (2010).
40. Zhang, F. & Liu, J. Label-free colorimetric biosensors based on aptamers and Gold nanoparticles: A critical review. *Anal. Sens.* **1** (1), 30–43. https://doi.org/10.1002/anse.202000023 (2021).
41. Shi, Z., Li, Q. & Mei, L. pH-Sensitive nanoscale materials as robust drug delivery systems for cancer therapy. *Chin. Chem. Lett.* **31** (6), 1345–1356. https://doi.org/10.1016/j.cclet.2020.03.001 (2020).
42. Coradeghini, R. et al. Size-dependent toxicity and cell interaction mechanisms of gold nanoparticles on mouse fibroblasts. *Toxicol. Lett.* **217** (3), 205–216. https://doi.org/10.1016/j.toxlet.2012.11.022 (2013).

Acknowledgements

We acknowledge prof Enrico Rampazzo for their support in performing DLS measurements.

Author contributions

J.W., S.G. and V.M. designed the work. J.W., S.G. and A.P. performed the scientific experiments and elaborated the data. V.M. supervised the work and data interpretation. J.W., S.G. and V.M. drafted the work. B.R., A.Z. and P.R. substantively revised the work and revised the bibliography. All authors reviewed the manuscript before submission.

Funding

Junjie wang's PhD grant was funded by the China Scholarship Council (CSC). Work Funded by the European Union - NextGenerationEU under the National Recovery and Resilience Plan (PNRR) - Mission 4 Education and research - Component 2 From research to business - Investment 1.1 Notice Prin 2022 - DD N. 104, February 2, 2022, from title Thermochemiluminescence-based nanoprobes for multiplex prostate cancer biomarkers in personalized medicine, proposal code 2022JL8JCM - CUP J53D23007570006

Competing interests

The authors declare no competing interests.

Additional information

Supplementary Information The online version contains supplementary material available at https://doi.org/10.1038/s41598-024-73624-0.

Correspondence and requests for materials should be addressed to V.M.

Reprints and permissions information is available at www.nature.com/reprints.

Publisher's note Springer Nature remains neutral with regard to jurisdictional claims in published maps and institutional affiliations.